8-2020

# The Effect of a Liquid Phase on Force Distribution During Deformation in a Granular System

Christopher R. Ladd
*Iowa State University*

Jacqueline E. Reber
*Iowa State University*, jreber@iastate.edu

# The Effect of a Liquid Phase on Force Distribution During Deformation in a Granular System


## Abstract

Two-phase systems, where one phase is solid and the other is fluid, are widespread in nature. Examples include reservoir rocks holding vital fluids like water or petroleum, slurries of partially crystallized magmas, fluids migrating along faults filled with fault gouge, and even the semibrittle crust. Previous studies of two-phase systems have shown that the fluid phase plays an important role in deformation localization and dynamics (e.g., Higashi & Sumita, 2009, https://doi.org/10.1029/2008JB005999; Reber et al., 2014, https://doi.org/10.1002/2014GL059832). Here, we present results from experiments investigating the influence of a fluid phase on force distribution in a granular media during simple shear. We use photoelastic polyurethane discs as the granular or solid phase and a linear viscous silicone as the fluid phase. The photoelastic property of the discs allows for direct observation and measurement of force magnitude and distribution. We compare the two-phase experiments to granular experiments without silicone. The addition and percentage of the fluid phase has a strong impact on the force distribution and the overall force chain orientations. In the two-phase system, the force chains form parallel to the shear plane and only rotate to the principal stress direction with an increase in strain. Locally, the fluid phase can support forces and terminate force chains over an extended period of time. Our results are in line with findings from numerical studies investigating the formation of slow slip events, proposing that these events are the result of dynamic interactions between solid and viscous phases.



## Disciplines

Geology | Geophysics and Seismology | Sedimentology

## Comments

This article is published as Ladd, C. R., Reber, J. E. (2020). The effect of a liquid phase on force distribution during deformation in a granular system. *Journal of Geophysical Research: Solid Earth*, 125, e2020JB019771. doi: 10.1029/2020JB019771.

JGR Solid Earth

RESEARCH ARTICLE
10.1029/2020JB019771

# The Effect of a Liquid Phase on Force Distribution During Deformation in a Granular System

**Christopher R. Ladd**[1] and **Jacqueline E. Reber**[1]

[1]Department of Geological and Atmospheric Sciences, Iowa State University, Ames, IA, USA

**Key Points:**
- The presence of a fluid phase affects the force distribution in a granular system during shear deformation
- The presence of a fluid phase changes the average force chain orientation and deformation localization
- The force can be supported for a limited time by the fluid phase

**Supporting Information:**
- Supporting Information S1

**Correspondence to:**
J. E. Reber,
jreber@iastate.edu

**Citation:**
Ladd, C. R., Reber, J. E. (2020). The effect of a liquid phase on force distribution during deformation in a granular system. *Journal of Geophysical Research: Solid Earth*, *125*, e2020JB019771. https://doi.org/10.1029/2020JB019771

Received 12 MAR 2020
Accepted 11 JUL 2020
Accepted article online 17 JUL 2020

**Abstract** Two-phase systems, where one phase is solid and the other is fluid, are widespread in nature. Examples include reservoir rocks holding vital fluids like water or petroleum, slurries of partially crystallized magmas, fluids migrating along faults filled with fault gouge, and even the semibrittle crust. Previous studies of two-phase systems have shown that the fluid phase plays an important role in deformation localization and dynamics (e.g., Higashi & Sumita, 2009, https://doi.org/10.1029/2008JB005999; Reber et al., 2014, https://doi.org/10.1002/2014GL059832). Here, we present results from experiments investigating the influence of a fluid phase on force distribution in a granular media during simple shear. We use photoelastic polyurethane discs as the granular or solid phase and a linear viscous silicone as the fluid phase. The photoelastic property of the discs allows for direct observation and measurement of force magnitude and distribution. We compare the two-phase experiments to granular experiments without silicone. The addition and percentage of the fluid phase has a strong impact on the force distribution and the overall force chain orientations. In the two-phase system, the force chains form parallel to the shear plane and only rotate to the principal stress direction with an increase in strain. Locally, the fluid phase can support forces and terminate force chains over an extended period of time. Our results are in line with findings from numerical studies investigating the formation of slow slip events, proposing that these events are the result of dynamic interactions between solid and viscous phases.

**Plain Language Summary** Systems containing a solid and a fluid phase are common in nature, including settings such as aquifers, petroleum reservoirs, water saturated fault sediments, and partially molten magmas. Previous work on two-phase systems has shown that the fluid phase is able to change deformation dynamics and increase deformation localization when compared to single-phase brittle systems. We conduct experiments using photoelastic discs as the solid phase and a silicone as the fluid phase. The photoelastic property allows for visualization and quantification of forces. We compare the two-phase experiments to granular experiments without silicone. Without silicone, force distributes along chains of discs that span the experimental apparatus. These force chains form in characteristic orientations that hold true throughout an experiment. The addition of the fluid phase significantly changes the force distribution. In two-phase experiments, force chains initially do not span the entirety of the experimental box and instead localize along a shear plane in the middle of the experiment. These force chain orientations change over time. We find that the fluid can support forces for extended periods of time. Our findings highlight the importance of the fluid phase on deformation in two-phase systems, which may have both economic and societal consequences.

## 1. Introduction

Geological systems are often complex and contain more than one material phase. Fluid-like and solid-like phases can coexist, leading to a complex deformation behavior. Such mixed systems can be found in the mantle where a mixture of magma and crystalline material is suspected (Cordonnier et al., 2012; Deubelbeiss et al., 2011; Lejeune & Richet, 1995), in the lower middle crust where despite all phases being below the solidus, different mineral phases exhibit different rheologies under the same pressure and temperature conditions (e.g., quartz deforms in a viscous manner, while feldspar fails brittle) (Evans et al., 1990; Handy, 1990; Mancktelow, 2008), in the upper crust where sedimentary rocks host a fluid phase such as hydrocarbons or water in their pore spaces (e.g., Maliva, 2016; Osborn et al., 2011; Soeder, 2018), or in surface processes such as landslides and liquefaction events (Brodsky & Kanamori, 2001; Goren et al., 2011; Iverson et al., 2000; Lejeune & Richet, 1995; Ross et al., 1987; Sibson, 1996). Most recently, such semibrittle materials have also been suggested to play a role in the formation of slow slip and tremor events (Beall

et al., 2019a; Birren & Reber, 2019; Fagereng & Sibson, 2010; Hayman & Lavier, 2014; Reber et al., 2015; Webber et al., 2018). The commonality of all these systems is that they have two phases where one is solid (brittle, strong) and the other one is fluid like (viscous, weak). The deformation of these two-phase systems is controlled by a multitude of factors including the rheology of the individual phases, the competency contrast between the phases, their spatial distribution, and their volume fraction (Handy, 1990; Holyoke & Tullis, 2006; Jammes et al., 2015; Jordan, 1988; Li et al., 2007).

Studies of poly-phase geological systems suggest that the fluid-like phase has a significant impact on the deformation behavior (Handy, 1990; Jammes et al., 2015; Pec et al., 2016). For a small amount of fluid-like phase, the bulk rheology is governed by the solid phase; the material is in a load-bearing framework with stresses distributed along solid-phase contacts and deformation mostly occurring via brittle failure or grain rearrangement in the solid phase. With an increase of fluid-like phase, the bulk rheology moves away from being dominated by the solid phase toward a rheology governed by the fluid-like phase. Whether both phases are actively deforming and how much of the fluid-like phase is necessary to dominate the deformation is mainly dependent on the competency or strength contrast between the two phases. For a large strength contrast, the fluid-like phase will dominate the rheology if it makes up 30% or more of the two-phase system (Holyoke & Tullis, 2006; Jordan, 1988). However, for a small strength contrast, both the solid and the fluid phases will accommodate deformation. Several theoretical mixing laws have been suggested to describe the dependence of the effective viscosity of the two-phase system on the concentration of the solid phase (Handy, 1994; Ji, 2004; Jordan, 1987; Roscoe, 1952).

Our knowledge of the stress distribution in such two-phase systems during deformation is quite limited as stress is not easily observable in most materials (e.g., Reber et al., 2020). Knowing the stress distribution and the location of stress peaks in a system is essential for understanding the material failure. The physics community has been interested in the force distribution in granular materials for many years (Cates et al., 1998; Herrmann et al., 1997; Liu et al., 1995; Majmudar & Behringer, 2005; Radjai et al., 1996), mainly because granular systems can be considered to be both fluids and solids. The stress distribution in a granular medium is only uniform in cases of perfect packing. As soon as the material shows disorder, the stress distribution is no longer uniform, and force chains develop. Force chains form when individual particles form bridges supporting stresses across the compressional direction (Cates et al., 1998; Peters et al., 2005). The formation and breaking of such force chains is associated with jamming in granular systems (Jaeger et al., 1996). As long as the force chains are intact, the system is jammed and behaves like a solid. With continuous deformation, these chains can break and rearrange, leading to stick-slip motion and a temporary "flow" of the system (Albert et al., 2001; Daniels & Hayman, 2008).

Physical experiments on mixed granular/viscous systems have shown that the deformation dynamics change significantly when a viscous phase is added to a granular frictional material (Geminard et al., 1999; Higashi & Sumita, 2009; Huang et al., 2005; Jang & Khonsari, 2005; Reber et al., 2014). Depending on the viscosity of the fluid, the effects range from a simple change in effective stress (low-viscosity fluids) (e.g., Mahabadi & Jang, 2017) to changes in deformation dynamics and localization (high-viscosity fluids) (e.g., Higashi & Sumita, 2009; Reber et al., 2014).

Here, we present results from physical experiments investigating the impact of a fluid phase on the force distribution in a two-phase material during simple shear deformation. By employing photoelastic materials, we document the force chain evolution in dry granular experiments as well as in experiments where the pore space is filled with a high-viscosity fluid. Our results show that the addition of a fluid phase has a significant impact on the force magnitude and distribution during deformation.

## 2. Method

Experiments are performed using a linear simple shear table consisting of two plates, where one plate is stationary, while the other plate is pulled at a constant rate of 0.337 mm/s (Figure 1a). This setup creates a discrete shear plane in the middle of the experiment where the two plates meet. The experimental material is confined by an aluminum frame to ensure the conservation of volume. During deformation, we record the overall force with a Chatillon DFS II piezoelectric force gauge and measure the displacement using a Celesco cable transducer. Both are measured at a rate of 10 Hz (Daniels & Hayman, 2008, 2009; Randolph-Flagg & Reber, 2020; Reber et al., 2014).

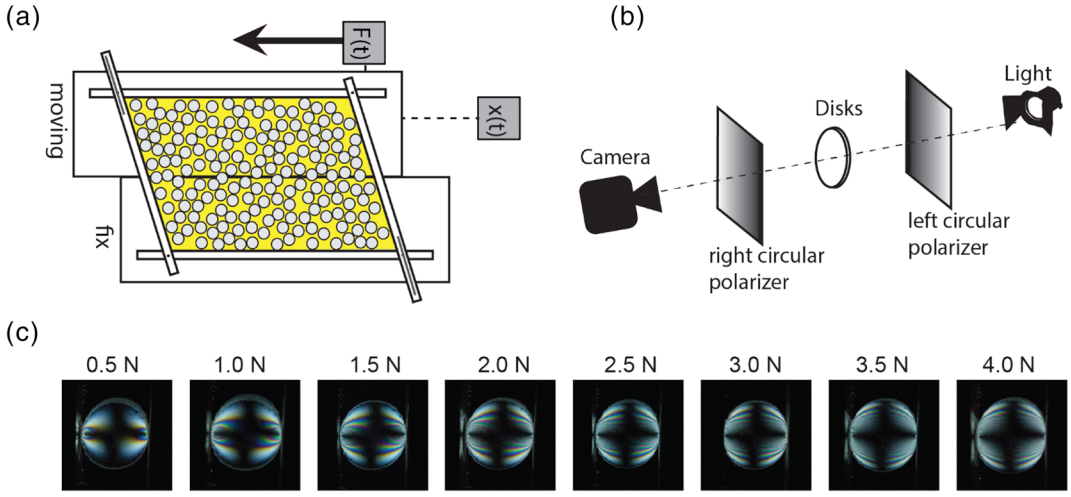


**Figure 1.** (a) Linear simple shear table exhibiting sinistral motion. Confining box shown as yellow-shaded region. (b) Schematic circular polariscope setup used for viewing the fringe patterns in the photoelastic discs. Circular polarizer = linear polarizer + quarter-wave plate. (c) Fringe pattern in a single disc with increasing force.

For the experiments, we chose a strain-rate convenient to attain high enough forces to visualize important variations between the two types of experiments over time. At the imposed strain rate ($3.74 \times 10^{-4}$ $s^{-1}$), the silicone behaves as a linear viscous fluid (Weijermars, 1986). The silicone viscosity is high enough to prevent leaking during the time it takes to conduct an experiment.

As model materials, we use 6.25-mm-thick circular polyurethane discs of two diameters (9 and 11 mm) as well as a linear viscous silicone (Dow Corning PDMS-DC SGM36) with a viscosity of $4 \times 10^4$ Pa s at room temperature. A single layer of 2,300–1,754 discs with a diameter of 9 mm and 884–674 discs with a diameter of 11 mm fills an area 90 cm long and 30 cm wide; the packing density is varied between 85% and 65% of the total experiment area. Having two disc sizes prevents perfect packing and instantaneous locking of the experiment during deformation. The silicone adheres to the polyurethane discs preventing free slip between the two materials.

The polyurethane discs are photoelastic. Photoelasticity is an optical material property, which transforms the transparent isotropic material into an anisotropic refractive (birefringent) material when subjected to a force (Hecht & Zajac, 1974). When stressed, the discs transmit light at varying intensities and exhibit sequential fringe patterns based on progressive force applied to each individual disc (Figure 1c) (Daniels et al., 2017). Fringe patterns form due to optical interference produced by the dependence of the refractive index of a material on the difference between principal stresses (Frocht, 1941). These fringe patterns can only be viewed using cross-polarized light (Figure 1b). Discs that support forces display fringes and appear bright, while discs that are not supporting forces remain black under cross-polarized light. We refer the reader to Daniels et al. (2017) for a short and comprehensive overview of photoelasticity and the construction of a polariscope.

To quantify the evolution and magnitude of these force networks or force chains, we take time-lapse photographs of the experiments from above with and without the second polarizer at 3-s intervals. To quantify the forces acting on each disc, we use a code developed by Daniels et al. (2017). The code, PEGS, uses the photoelastic images to calculate contact forces based on the fringe pattern displayed by each disc. The light intensity $I$ at any location in the material can be calculated using the following equation:

$$I = \sin^2 \frac{\pi(\sigma_1 - \sigma_2)}{F_\sigma}, \tag{1}$$

where $F_\sigma$ is the stress optic coefficient that accounts for the reactional property of the material to stresses (Frocht, 1941). Only two stresses are considered, $\sigma_1$ and $\sigma_2$, because the material is only deformed in two dimensions. The stress optic coefficient $F_\sigma$ is a material constant and can be calculated by

$$F_\sigma = \lambda / Ct, \tag{2}$$

where $C$ is an optical property of material measured in Brewsters (Figure 6a), $\lambda$ is the wavelength (m) of the light source used for the experiments, and $t$ is the thickness of the material (Puckett, 2012).

In addition, the stress optic coefficient can be determined empirically by using a diametric load test. We subject a disc to a known force and record the corresponding fringe number (Figure 1c). The fringe number is counted from the edge to the center of a disc; each dark band and each light band is worth 0.5 fringes so that a pair of light and dark fringes is equal to one fringe (Daniels et al., 2017; Puckett, 2012). With the force and fringe number, the stress optic coefficient can then be determined in the following manner (Puckett, 2012):

$$F_\sigma = \frac{4F}{\pi R N_{\text{Fringe}}}. \tag{3}$$

$F$ is the force ($N$) applied to the disc, $R$ is the radius (m) of the disc, and $N_{\text{Fringe}}$ the fringe number. We record $N_{\text{Fringe}}$ for increasing forces and calculate $F_\sigma$ using the slope of the line produced by Equation 3. We obtain $F\sigma \approx 123$ kg/s$^2$. Once $F\sigma$ is known, the contact forces in each disc can be calculated by using Equation 1.

To calibrate the fringe matching portion of the code, the light intensity difference between sequential pixels in an image ($G^2$) needs to be known. $G^2$ is used as a contact verification method and for creating the synthetic force images to match to experimental fringe images. A sufficient change in light intensity determined by $G^2$ must be attained for a contact between two discs to be validated. Once contacts are validated, contact forces can be calculated. To calibrate $G^2$ for force calculation purposes, we input the $F_\sigma$ value of the material into a separate code from the PEGS (photoelastic grain solver) package. This code creates synthetic photoelastic response images to probe the appropriate $G^2$ scaling. For each force, the $G^2$ vaules are obtained from the respective synthetic image (see Figure S1 in the supporting information). The relationship calculated here between $G^2$ and force on synthetic images allows forces to be found based on fringe image matching. Changing the $F_\sigma$ value changes sythetic fringe counts, so having the correct $F_\sigma$ value is vital to calculating forces correctly.

The first step when using PEGS is to input two images, the cross-polarized image with the photoelastic response of the discs and a nonpolarized image for finding the disc positions. From the input images, the code will first find the location of each disc. In a second step, the individual discs are cropped, and their position is matched to the photoelastic image. Next, disc brightness and position are used to find neighboring discs experiencing force. Force chain traces are plotted based on the neighbors found. Force calculation at the individual disc level is solved based on brightness and fringe number. Last, all computed discs are combined into a full synthetic force image. See Daniels et al. (2017) for a detailed description of the code.

To obtain the orientation of the force chains at various strains, we use the force chain traces produced by PEGS. We employ FracPaQ, a fracture orientation evaluation code developed by Healy et al. (2017), to obtain the orientations of individual force chain segments as well as the average of all chains.

### 2.1. Balancing Forces

To validate the calibration of the code, we compare the calculated total force in an experiment to the force recorded by the force gauge during deformation. This validation is done for granular experiments as well as for two-phase experiments where the pore spaces between the discs are filled with a fluid. For a meaningful comparison between the calculated and measured forces, we subtract the force required to move the empty experimental table (background force) from the force measured during the experiment (Figures 2 and 3, red line). Because the images employed for force calculations do not capture the entire experiment, the calculated forces have to be scaled. The images used for force calculation capture between 15% and 30% of the total table area (Figures 2b and 3b). Once the measured bulk force and the calculated force are corrected, we can compare the two independent force measurements. In the granular experiment, the average difference between the total and the calculated force is 0.48 N with a standard deviation of 0.59 N (Figure 2c). This is 2.5% of the overall force in the granular experiment. The average difference between the total and the calculated force of the two-phase experiment is 0.46 N, with a standard deviation of 0.645 N (Figure 3c). The error in the two-phase experiments is <1% of the total force.

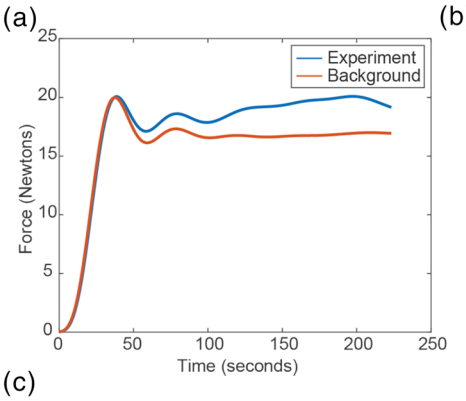


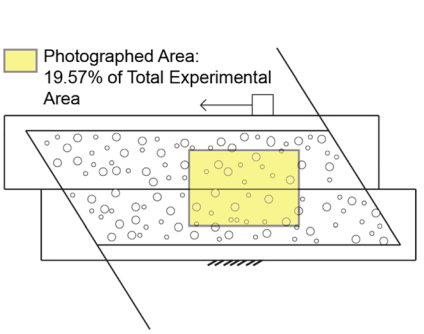


(c)

| Strain | γ = 0.004 | γ = 0.02 | γ = 0.05 | γ = 0.075 | γ = 0.08 | γ = 0.10 | γ = 0.125 |
|---|---|---|---|---|---|---|---|
| Total Force (Measured at Gauge) | --- N | 18.15 N | 18.08 N | 19.21 N | 19.66 N | 19.88 N | 19.16 N |
| Background Force | --- N | 17.4 N | 16.79 N | 16.63 N | 16.75 N | 16.80 N | 16.94 N |
| Remainder (Total - Background) | --- N | 0.75 N | 1.29 N | 2.58 N | 2.91 N | 3.08 N | 2.22 N |
| Force in Area Photographed (19.57% of Remainder) | --- N | 0.147 N | 0.252 N | 0.505 N | 0.570 N | 0.603 N | 0.435 N |
| Force Calculated by Code | 0.213 N | 0.290 N | 0.171 N | 0.564 N | 0.708 N | 1.981 N | 1.653 N |
| Difference (Measured - Calculated) | --- N | - 0.143 N | 0.081 N | - 0.059 N | - 0.138 N | - 1.378 N | - 1.218 N |

**Figure 2.** (a) Total force measured during a granular experiment (blue) and background force from the table with no grains (red). (b) Representation of area photographed during this granular experiment and used by the code for calculating forces. In this experiment, the yellow box represents 19.57% of the table area. (c) Table for comparing measured and calculated forces. The last row compares the force measured by the gauge to the force calculated by the code.

## 3. Results

In order to isolate the influence of the fluid phase on the stress distribution during deformation, we performed 10 experiments in the absence of the fluid phase for comparison with 10 two-phase experiments. Both types of experiments have a packing density of 85%. The only difference between the two sets of experiments is the addition of the fluid phase; the strain rate, number of discs, and shear box dimensions are held constant. Experiments are run until discs begin to pop out of plane, usually around a shear strain of $\gamma = 0.15$ for granular experiments and $\gamma = 0.25$ for two-phase experiments.

Qualitatively, there are evident differences between the two sets of experiments. In the granular experiments, force chains form a framework pattern spanning the width of the experimental box and distributing the force to the boundaries of the experimental box (Figure 4). This behavior is common in granular materials and has been observed in a multitude of different experiments (Cates et al., 1998; Daniels & Hayman, 2008; Majmudar & Behringer, 2005). We observe an increase in number of force chains with continuous deformation (Figure 4). Furthermore, the discs appear brighter with an increase in strain and therefore stress. In comparison to the granular experiments, the experiments containing a viscous fluid show force chain patterns that differ in several aspects (Figure 4). Overall, more discs appear bright even at the onset of deformation. While some force chains extend to the boundaries, strong force chains can be observed close to the center of the experiment. Discs that are close to the shear plane imposed by the experimental table are highly stressed, while discs away from the shear plane show less stress. As shear strain increases, the force chains grow toward the boundaries of the experimental box. Also contrasting the granular

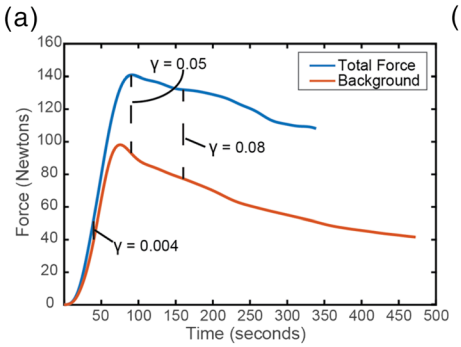


(c)

| Strain | γ = 0.004 | γ = 0.01 | γ = 0.05 | γ = 0.075 | γ = 0.08 | γ = 0.10 | γ = 0.125 |
|---|---|---|---|---|---|---|---|
| Total Force (Measured at Guage) | 51.61 N | 77.56 N | 140.80 N | 134.20 N | 131.80 N | 130.60 N | 124.40 N |
| Background Force | 40.77 N | 60.92 N | 90.85 N | 80.71 N | 76.12 N | 72.85 N | 63.35 N |
| Remainder (Total - Background) | 10.84 N | 16.64 N | 49.95 N | 53.49 N | 55.68 N | 57.75 N | 61.05 N |
| Force in Area photographed (18.89% of Remainder) | 2.05 N | 3.14 N | 9.44 N | 10.10 N | 10.51 N | 10.91 N | 11.53 N |
| Force Calculated by code | 1.57 N | 3.44 N | 7.61 N | 10.03 N | 10.35 N | 10.09 N | 11.36 N |
| Difference (Measured - Calculated) | 0.48 N | - 0.30 N | 1.83 N | 0.07 N | 0.16 N | 0.82 N | 0.17 N |

**Figure 3.** (a) Total force measured during a two-phase experiment (blue) and background force from table with only silicone present (red). (b) Representation of area photographed during this two-phase experiment and used by code for calculating forces. In this experiment, the yellow box represents 18.89% of the table area. (c) Table for comparing measured and calculated forces. The last row compares the force measured by the gauge to the force calculated by the code.

experiments, the force chains change in intensity along their lengths. Discs away from the shear plane are less stressed and form fewer fringes than discs close to the shear plane.

Another difference between granular and two-phase experiments can be seen in the measure of the bulk force (Figures 2a and 3a). The granular experiments load quickly before a small drop in force occurs. The

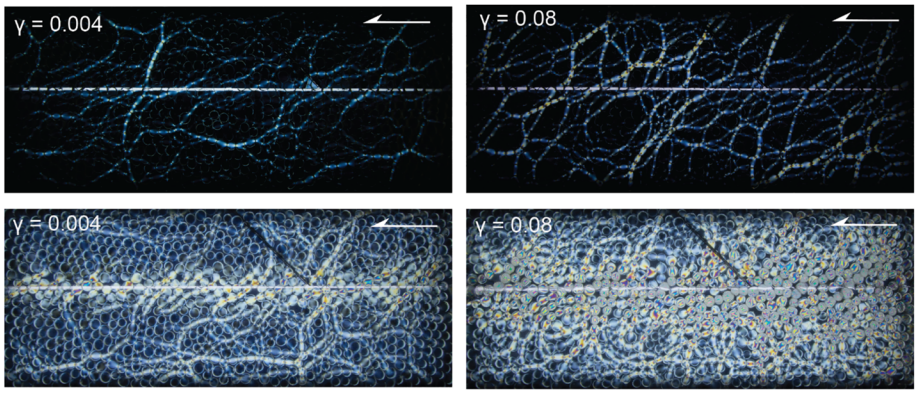


**Figure 4.** Force chain networks in granular experiments (top row) and two-phase experiments (bottom row) at low and high strains. The bright line in the middle of each photographs marks the shear plane imposed by the experimental apparatus.

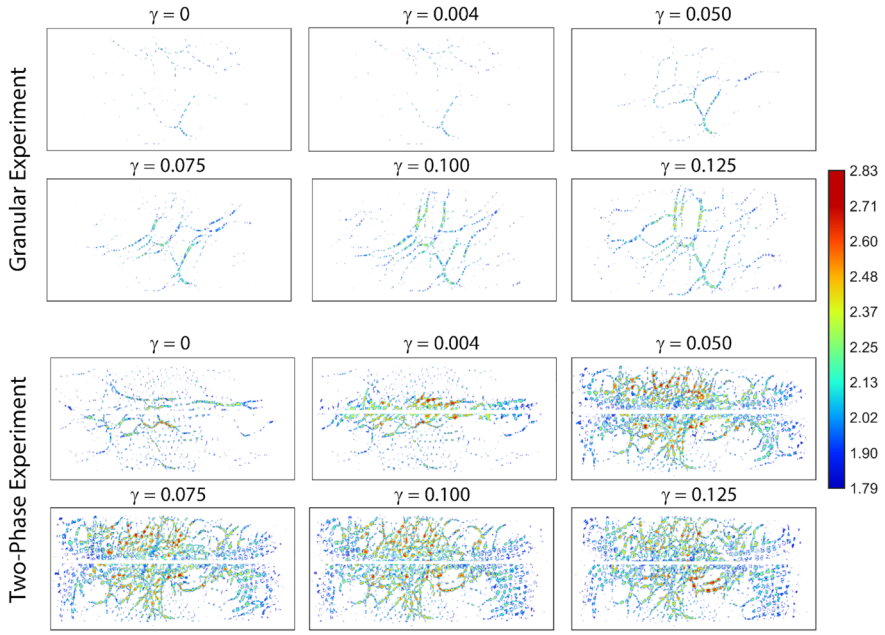


**Figure 5.** Force chain distribution and force magnitude for a typical granular (top) and two-phase (bottom) experiment with increasing strain. Colors correspond to forces in N.

force then increases throughout the rest of the experiments with minor oscillations. The two-phase experiments also exhibit a quick loading period, but then force gradually decreases throughout the rest of the experiment. We attribute this decrease in force to the lubrication in the experiment due to the fluid phase (Reber et al., 2014).

### 3.1. Force Chain Evolution

During the course of a granular, experiment the formation and breaking of several force chains can be observed. Overall, we see an increase in the number of force chains with increasing strain (Figure 5). While we would expect to find no force chains at the onset of the experiments, we do observe some minor force chains developing during the setup of the experiment. They are a side effect of the experimental setup and fail as soon as deformation sets in (Figure 5, $\gamma = 0$). At a shear strain of $\gamma = 0.004$, some new force chains have formed. The maximum recorded force in an individual disc is 2.25 N. With increasing strain, force chains increase in number and in brightness, indicating that they are supporting higher forces. At $\gamma = 0.075$, the maximum force measured in any force chain is 2.50 N. At $\gamma = 0.100$, there are multiple force chains supporting a maximum force of 2.50 N. At $\gamma = 0.125$, some of the force chains have failed and are supporting less force.

Comparing the granular experiments to the two-phase experiments, we observe an overall higher force in the two-phase experiments reaching up to 2.83 N in an individual disc (Figure 5). Similar to the granular experiments, we see some minor force chains that are due to the experimental setup (Figure 5, $\gamma = 0$). At the onset of shearing, new chains form and localize along the shear plane. Discs located in close proximity to the shear plane experience the highest forces, while discs close to the edge of the experimental box are undeformed. At $\gamma = 0.050$, the force chains have grown in length away from the shear plane. Discs at the shear plane appear to be experiencing lower forces but are actually so highly strained that light does not pass efficiently through the discs for accurate force calculation. Above $\gamma = 0.050$, the force chains stop growing toward the edges of the experimental box. In contrast to the granular experiments, force chains in two-phase experiments do not suddenly fail along their whole length. Instead, discs slipping at the shear plane can lead to a reduction of force in a chain, but as soon as that chain is again in contact with another disc at the shear plane, force will increase once more in the chain.

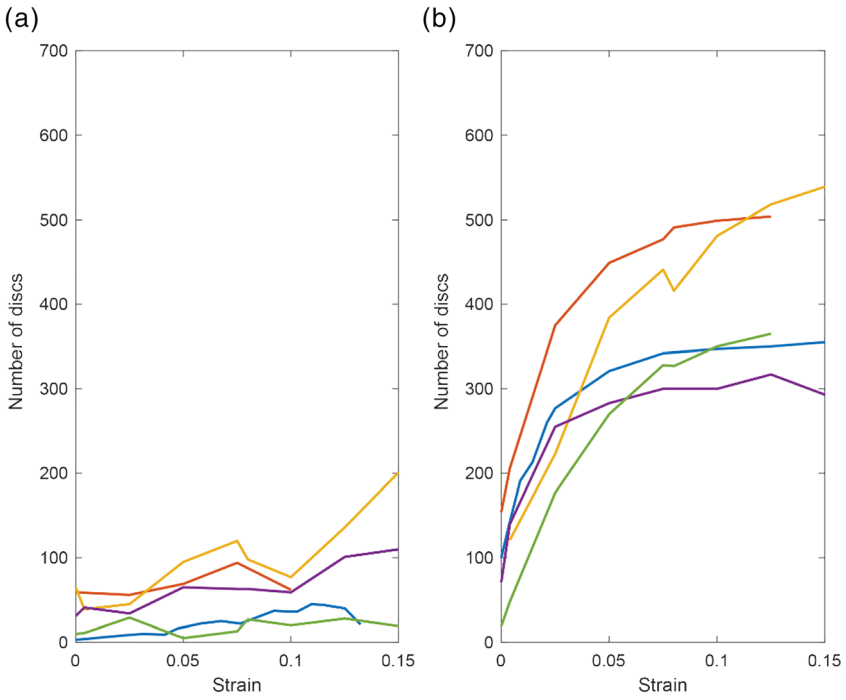


**Figure 6.** Number of discs with a brightness above 1 N of force plotted against strain. (a) Five granular experiments and (b) five two-phase experiments. Colors represent individual experiments.

To illustrate this difference in the force chain failure dynamics, we count the number of discs supporting >1 N of force. In the granular experiment, the number of discs experiencing >1 N of force increases with strain in a nonsmooth fashion (Figure 6a). This sawtooth pattern is evidence of the formation and failure of force chains, where failures correspond to a decreasing number of discs reaching the threshold force.

The number of discs experiencing a force larger than 1 N in two-phase experiments differs from the number in granular experiments (Figure 6). At $\gamma = 0$, many of the discs already show a force >1 N. As soon as deformation sets in, we observe a rapid increase in the number of discs with a force above 1 N. Between $\gamma = 0$ and $\gamma = 0.025$, the largest increase in discs displaying force above 1 N occurs. At $\gamma = 0.05$, the number of discs above the threshold begins to level off and eventually approximate a steady state. At this point, more than 50% of the discs in the experiments experience large enough forces to pass above the threshold level. In comparison, fewer than 20% of all discs in the granular experiments reach strains high enough to pass above the threshold level at any point in the experiments. The shape of the curves from the two-phase experiments further indicates that force chains only fail temporarily, since there are few decreases in the number of discs above the threshold force.

Zooming in on an individual force chain, we observe a difference in behavior between the granular and two-phase experiments. In granular experiments, all force supporting discs are in contact with at least two other discs. This leads to force chains that span the entire width of the experimental box. Discs in contact with only one other disc do not support any force (Figures 7a and 7b, circled disc). This is in contrast to the observations in two-phase experiments where it is not uncommon to see discs that show fringe patterns, which are in contact with only one other disc (Figures 7c and 7d). The disc investigated in Figure 8 shows one real contact to a neighboring disc (circled in blue). The other three contacts (circled in purple, yellow, and orange) show ghost contacts that are bridged by the fluid. This means that the disc is not in direct contact with more than one other disc, but instead, the stress is transferred via the fluid phase. During the life of the experiment, this disc experiences an increase followed by a decrease in force where individual contacts to other discs contribute various amounts of force (Figure 8). This normal force is transmitted through the fluid as a pressure in the fluid. The fluid around this specific disc was able to support an average force of 0.65 N for over 60 s.

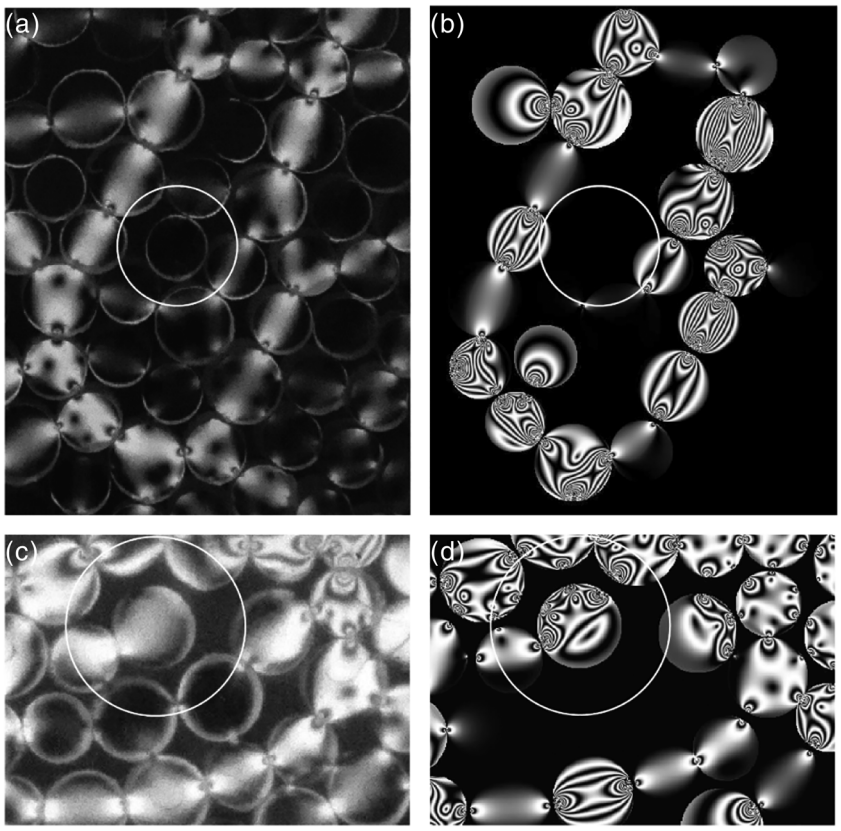


**Figure 7.** Photo of (a) granular experiment and (c) two-phase experiment under cross-polarized light. Circled disc is in contact with only one other disc. (b and d) Synthetic force image produced by PEGS code showing the same disc assembly. Note that larger discs have a diameter of 11 mm.

### 3.2. Force Chain Orientations

To quantify the orientation of the individual force chains, we obtain the orientation of individual segments of each force chain. A segment is defined as the line from the center of one disc to the center of the next disc involved in a force chain. The azimuthal value of each segment is then plotted in a rose diagram using 10° interval bins (Figure 9). Colors represent the azimuth of each bin. Bin sizes represent a percentage of the total number of force chain segments counted in the experiment at a given strain. To compare different experiments to each other, we calculate and plot the average force chain orientation (Figure 10). For reference, the shear plane of the experimental apparatus aligns with the 90–270° orientation.

Force chains in a granular experiment develop in two major orientations, 15° and 80° at low strain and shift slightly to 15° and 75° at higher strain (Figures 9a and 9b). The average force chain orientation nearly bisects the two major orientations, plotting at 38° at low strain and at 34° at high strain. Very few chains form with an orientation between 90° and 180°.

At low strain, force chains in a two-phase experiment develop in a dominant orientation between 70° and 100°. The average force chain orientation falls within that range with 79° (Figure 9c). At high strains, there are no obvious dominant orientations (Figure 9d). The average force chain orientation of this high strain two-phase experiment is 56°.

By amassing average force chain orientations of all 20 experiments, we find that the average orientations differ between granular and two-phase experiments as well as between low and high strains (Figure 10, Table 1). The average angle of the force chain segments from all the low strain granular experiments is 58° (Figure 10a). At an increased strain, the average angle decreases to 54° (Figure 10b). The two-phase low strain experiments have an average angle of 78° (Figure 10c), while at a high strain, the average angle decreases to 54° (Figure 10d).

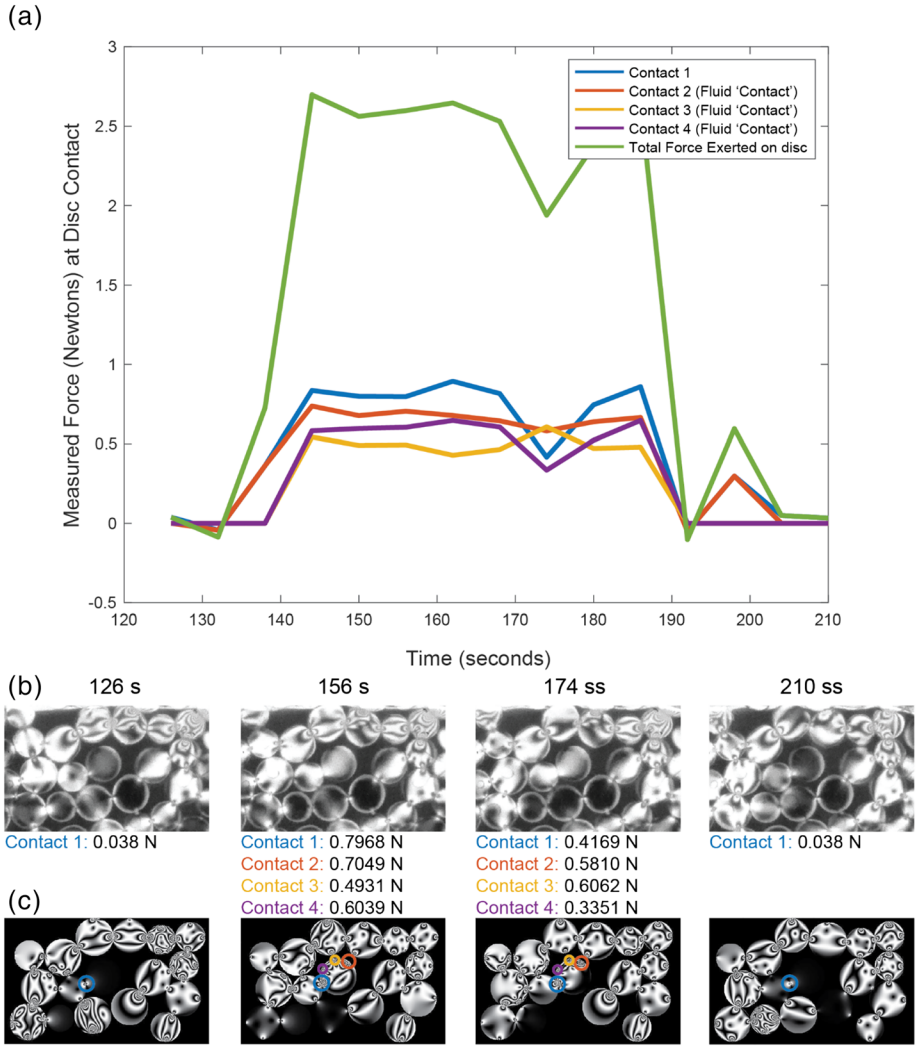


**Figure 8.** Force evolution of circled disc in Figures 7c and 7d through time. (a) Time versus force on four different disc contacts. (b) Photographs of experiment showing the same disc assembly at 126, 156, 174, and 210 s since the onset of deformation. (c) Calculated fringe patterns of the same disc assembly. Colored circles indicate different force contacts.

We use the Kullback-Leibler (KL) divergence method to quantify the significance of difference between the different experiments. The KL divergence method can be used to compare data generated under different conditions for similarities and differences (Kullback & Leibler, 1951). KL divergence values are dimensionless with larger numbers corresponding to more difference between distribution densities. A statistically significant difference is assigned based on the data set being used. Our KL data have two size distributions on the order of 0.1 and 0.01. Because of the order of magnitude difference for our data, a difference of 0.1 is considered as being statistically significant.

When comparing the low strain to the high strain experiments in a granular setting, the divergence is 0.098. In two-phase experiments, the comparison between low and high strain leads to a KL divergence of 0.138. Figure 10 shows that the difference between average force chain orientations in two-phase experiments between low and high strain is large, while the difference between low and high strain in the granular experiments is small, which is reflected in the KL divergence numbers. When we compare granular experiments to two-phase experiments at low strains and high strains, we obtain KL divergence numbers of 0.178 and 0.151, respectively. The force chain orientations between the two types of experiments are significantly different at both strains (Table 1).

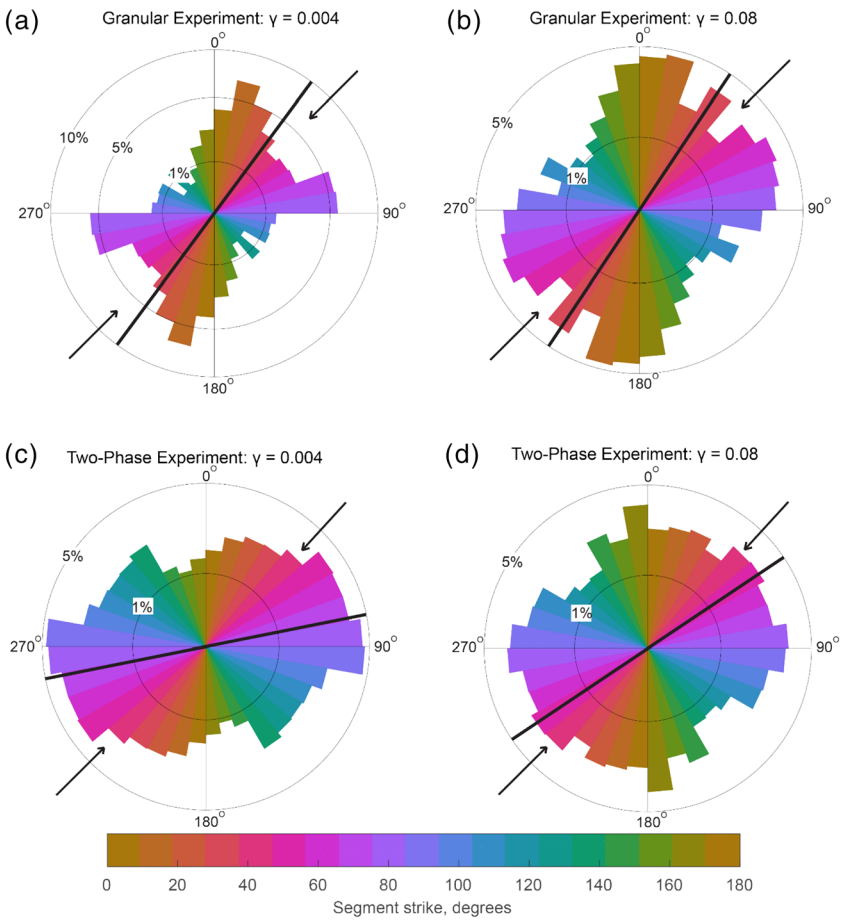


**Figure 9.** Rose diagrams showing force chain orientations. Colors represent azimuth values. (a) Granular experiment at low strain, $\gamma = 0.004$. (b) Granular experiment at $\gamma = 0.08$. (c) Two-phase experiment at $\gamma = 0.004$. (d) Two-phase experiment at $\gamma = 0.08$. Arrows represent the principal stress orientation. The shear plane of the experimental apparatus aligns with the 90° orientation.

### 3.3. Effect of Varying Clast Proportion in Two-Phase Experiments

To investigate the effect of the packing density on the force chain development in the two-phase experiments, we vary the clast proportion between 85% and 65%. We keep the ratio of small to large discs constant. Independent of the packing density, force chains develop in a similar manner. We observe a strong localization of deformation at the onset of deformation. With increasing deformation, the force gets distributed away from the shear plane. While at a high clast concentration (packing density of 85%, Figures 11a–11d), the force chains grow until they reach the boundary of the experimental box, this cannot be observed for lower clast concentrations (Figures 11e–11l). With a decrease in packing density, the deformation remains localized.

## 4. Discussion

The experiments presented here belong to the category of granular photoelastic experiments, which have been used to study deformation dynamics in granular materials before (e.g., Clark et al., 2012; Daniels et al., 2017; Daniels & Hayman, 2008; Iikawa et al., 2016; Mahabadi & Jang, 2017; Majmudar & Behringer, 2005; Uenishi & Goji, 2018). The experiments are designed in an analytical framework (Hooke, 1968; Paola et al., 2009; Reber et al., 2020). This is in contrast to experiments designed in an analogy-based framework where a direct scalability to the natural prototype can be achieved by applying a simple algebraic operation. Experiments in an analytical framework do not have to fulfill such a stringent scaling, but they still need to capture enough of the dynamics observed in the prototype to serve as a

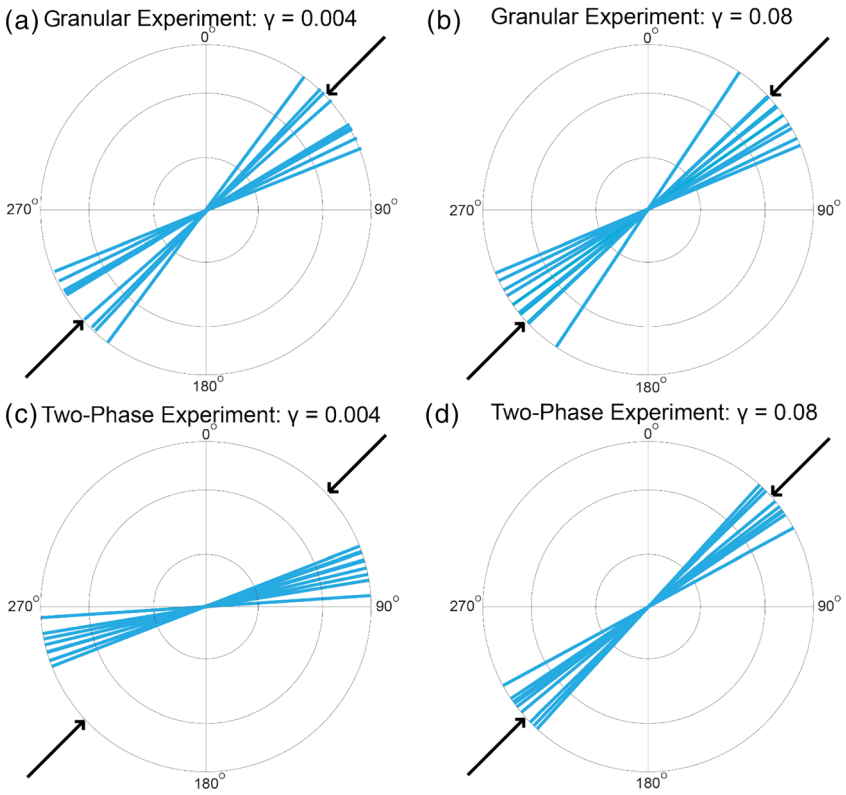


**Figure 10.** Average force chain orientations of granular and two-phase experiments at low and high strains. The black arrows represent the principal stress direction. Like the rose diagrams, the top of the chart represents 0°. (a) Average force chain orientations of 10 low strain granular experiments. (b) Average orientations of the same granular experiments at higher strain, $\gamma = 0.08$. (c) Average orientations of 10 low strain two-phase experiments. (d) Average orientations of the same 10 two-phase experiments at higher strain, $\gamma = 0.08$.

plausible testing ground to investigate the problem at hand. Even though the here presented experiments cannot be simply scaled, they allow us to make *in situ* observations on how the presence of the fluid phase impacts the distribution of force during simple shear in a granular media, which in all likelihood is similar to processes observed in nature (Fagereng & Sibson, 2010; Handy, 1990; Hayman & Lavier, 2014).

Even though most natural two-phase systems are expected to be three-dimensional, our experiments investigate the problem in two dimensions. This simplification allows for a direct observation of the force chains and their associated stress fluctuations through time. One disadvantage of conducting the two-phase experiments in 2D is that the fluid phase can be easily separated into nonconnected pores, especially in pores created by three surrounding discs. This is, however, not an exclusively two-dimensional problem but could also affect a system in 3D and has a direct effect on the pore fluid pressure during deformation as equilibration of the pressure can be inhibited in nonconnected pores (Aharonov et al., 1997; Goren et al., 2011).

**Table 1**
*Overall Average Angle of Force Chains in the Respective Experiments at Low and High Strain and KL Divergence Values Between Respective Experiments*

| **Force chain angles** | | | |
|---|---|---|---|
| Av. low strain G | Av. high strain G | Av. low strain TP | Av. high strain TP |
| 58 | 54 | 78 | 54 |
| **KL divergence** | | | |
| Low strain G – high strain G | Low strain TP – high strain TP | Low strain G – low strain TP | High strain G - High strain TP |
| 0.098 | 0.138 | 0.178 | 0.151 |

Abbreviations: G = granular experiments, TP = Two-phase experiments.

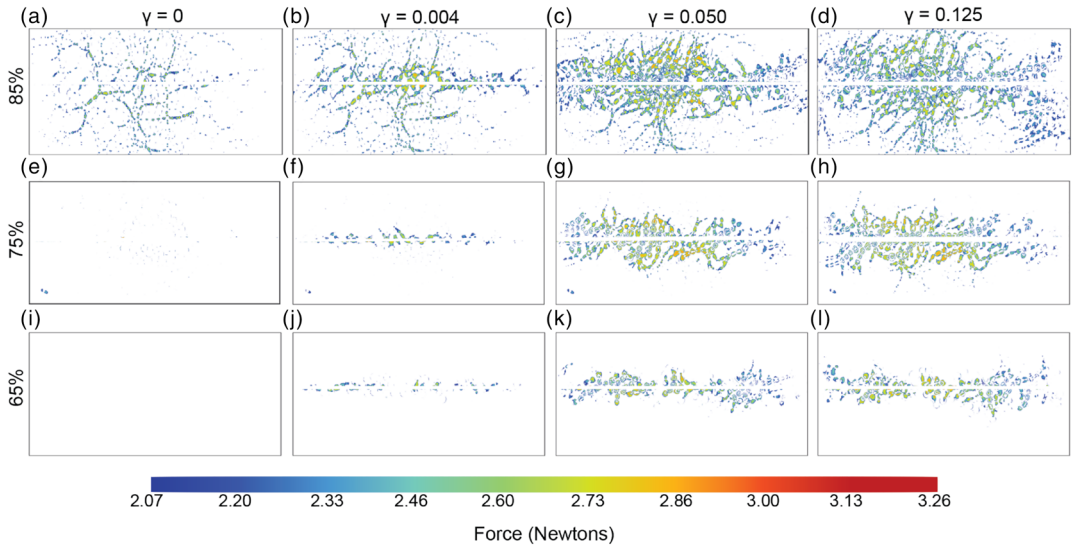


**Figure 11.** Force chain distribution and force magnitude of two-phase experiments with a clast concentration of 85% (top row), 75% middle row, and 65% bottom row.

The grain shapes in the here presented study are idealized to investigate the influence of the fluid phase. Discs of two different diameters are distributed randomly to inhibit perfect packing, and therefore locking, during deformation which occurs in single-size granular systems (Kennedy, 2006). Using discs also minimizes shape effects that would lead to uneven stress distributions (e.g., Ju et al., 2018). Even though grain shape and orientation, as well as the distribution of the phases, are important parameters that can determine how a two-phase system deforms (Handy, 1990; Jordan, 1987; Montesi, 2013), they are currently not accounted for in our experiments.

Similar to the findings presented in Reber et al. (2014) where they investigate the impact of fluid viscosity on the deformation dynamics in a two-phase system, we observe that the addition of the fluid phase impacts the deformation localization. While we do not monitor the motion of individual discs, we see an increase in the localization of the force. This localization increases with a decrease in clast concentration. All the experiments with a fluid phase show that the force is strongly localized around the shear plane of the experimental table at the onset of deformation. With an increase of strain, the deformation becomes more distributed (Figure 11). A similar behavior has also been documented in a numerical study of a quartz and feldspar mixture at semibrittle crustal conditions (Jammes et al., 2015). The results presented here suggest that the fluid-like phase can impede deformation in the solid phase, but only for a limited amount of time. Eventually the system will equilibrate and the solid phase will be supporting the majority of the force, leading to a widening of the shear zone (Figure 5). During this initial localization of deformation in the two-phase experiment, the system is not able to support shear forces, especially at lower disc concentrations (Figure 11). This is in contrast to granular systems where the force chain networks span the entire experiment and provide resistance to shearing (Howell et al., 1999). This difference in behavior has direct implications for the stability of a two-phase system during deformation.

While we do not monitor the pore pressure in the experiment, we observe that the fluid is able to exert force onto the discs (Figures 8 and 11). Our results indicate that force chains in two-phase experiments are less likely to fail (Figures 5 and 6) as the fluid phase can temporarily support forces. The fluid viscosity has a large effect on how much force can be supported and over what time scales. For fluids with a low viscosity, such as water, the viscous phase leads only to a slight increase in number of contact forces (Mahabadi & Jang, 2017).

This temporary support of force in a weak phase can also be observed in numerical models investigating the deformation dynamics of a subduction mélange (Beall et al., 2019b). Beall and colleagues found that stress amplifies within the stronger material due to jamming and the formation of force chains. During these jammed periods, the fluid-like phase can exert enough force onto the solid phase to provide a potential explanation for fracturing of brittle materials in the presence of overall moderate fluid pressures. A significant

difference between these numerical simulations and the here presented experiments is the ratio between the two phases. Beall et al. (2019b) investigate the deformation of a two-phase system with a ratio of the slid-like to fluid-like phases between 0.3 and 0.64. The numerical study by Beall et al. (2019b) employs significantly fewer but larger clasts. They observe a force chain orientation that is subparallel to the principal stress orientation, while the force chains in our two-phase experiments start out at an orientation parallel to the shear plane and only over time become subparallel to the principal stress orientation.

To compare the bulk rheology of the two-phase experiments to the bulk rheology used by Beall et al. (2019b), we calculate the effective viscosity of the composite material following the Marone-Pierce-Katano model (Barnes, 2003). This model calculates the effective viscosity of a mixture of a Newtonian fluid phase and a densely packed granular material

$$\eta_{\text{eff}} = \eta_0 \left(1 - \frac{\phi}{\phi_m}\right)^{-2}, \tag{4}$$

where $\eta_0$ is the viscosity of the fluid phase, $\phi$ is the disc fraction, and $\phi_m$ is the maximum disc fraction. With a maximum disc fraction in the experiments of 0.907 (Kennedy, 2006), the two-phase experiments have an effective viscosity of $7.17 \times 10^6$ Pa s. Normalizing the effective viscosity with the viscosity of the fluid phase reveals that the bulk viscosity of our experiments is consistent with the theoretical mixing model without jamming proposed by Roscoe (1952). Similar to our findings, results obtained by Beall et al. (2019b) also plot along the Roscoe without jamming mixture law for clast ratios between 0.3 and 0.64.

While the numerical study of Beall and the here presented experiments use generalized clast geometries, Webber et al. (2018) base their numerical model that investigates the effect of a two-phase system on deformation dynamics on observations form nature. They use the distribution of the two phases on observations from a subduction mélange (Chrystals Beach Complex, NZ), where the distribution between the two phases is 70% competent clasts and 30% weak matrix. They report cyclic formation of strain transients during deformation, which can be compared to slow slip events in nature. The potential of slow slip events being governed by the interaction of a brittle/solid phase with a fluid/viscous phase has been suggested by numerous authors (e.g., Beall et al., 2019a; Fagereng & Sibson, 2010; Lavier et al., 2013; Reber et al., 2014, 2015; Webber et al., 2018). The idea behind this is that an altering clast- or matrix-supported rheology can lead to either fast slip (earthquakes, clast-supported rheology) or slow slip events (matrix-supported rheology). While we did not monitor slip dynamics in our experiments, we measured how much force the weak phase can support over time. The presented findings are in line with results obtained from numerical simulations (Beall et al., 2019a, 2019b; Webber et al., 2018) and strengthen the argument that the presence of a weak phase has the potential to distribute forces more evenly leading to the potential of creep and the formation of slow slip events.

## 5. Conclusions

Displacement, force, and force chain distributions are measured during simple shear experiments of granular and two-phase systems. The photoelastic quality of the granular material allows for *in situ* observation of stress distribution during deformation within each system. The addition of a fluid phase to a granular system has an impact on multiple aspects of the deformation:

1. In the granular experiments, force chains build a load-bearing framework that spans the entire experimental chamber from the onset of deformation. In the presence of a fluid phase, no load-bearing force chain network develops at the onset of deformation, reducing the ability of the system to withstand shear forces. In two-phase systems, the force chains initially localize along the shear plane imposed by the experimental apparatus and terminate before reaching the boundaries. With an increase in strain, the force chains, however, grow longer, and deformation becomes more distributed.
2. The clast concentration in two-phase systems governs the degree of force localization. This localization is more pronounced in experiments with a low clast concentration.
3. In granular experiments, force chains form predominantly parallel to the principle stress direction. This overall force chain orientation is independent of strain. In the two-phase experiments, the mean

orientation of the force chains changes with increasing deformation from an orientation subparallel to the shear direction to an orientation approximating the principle stress direction.

4. Force chains grow in number and magnitude in a nonlinear fashion as stress increases in the granular experiments, where chains break and rearrange continuously. In the two-phase experiments, the forces are distributed more evenly, leading to an increasing number of discs supporting force with an increase in strain.
5. The results from two-phase experiments show that force can be supported for a limited time by the fluid phase.

The results from the experiments show that the presence of a fluid phase in a granular material has a significant impact on the force distribution within the system. This can lead to a change in the ability to support shear stresses during deformation, which may have a direct impact on extraction of natural resources, stability of faults, or deformation localization and dynamics in the middle crust.

## Data Availability Statement

The raw data used for this publication can be accessed via the Iowa State University data repository (https://doi.org/10.25380/iastate.12103989).

**Acknowledgments**

is made to the Donors of the American Chemical Society Petroleum Research Fund for support of this research. We thank Karen Daniels and Jonathan Kollmer for help with their force codes, Jon Coy for help with ImageJ, and Robert Hartmann for the cutting of the photoelastic discs. Thoughtful and helpful suggestions and comments by Matej Pec and an anonymous reviewer are greatly acknowledged.

## References

Aharonov, E., Spiegelman, M., & Kelemen, P. (1997). Three-dimensional flow and reaction in porous media: Implications for the Earth's mantle and sedimentary basins. *Journal of Geophysical Research*, *102*(B7), 14,821–14,833. https://doi.org/10.1029/97JB00996

Albert, I., Tegzes, P., Albert, R., Sample, J. G., Barabasi, A. L., Vicsek, T., et al. (2001). Stick-slip fluctuations in granular drag. *Physical Review E*, *64*(3), 031307. https://doi.org/10.1103/PhysRevE.64.031307

Barnes, H. A. (2003). A review of the rheology of filled viscoelastic systems. *Rheology Review*, 1–36.

Beall, A., Fagereng, A., & Ellis, S. (2019a). Fracture and weakening of jammed subduction shear zones, leading to the generation of slow slip events. *Geochemistry, Geophysics, Geosystems*, *20*, 4869–4884. https://doi.org/10.1029/2019GC008481

Beall, A., Fagereng, A., & Ellis, S. (2019b). Strength of strained two-phase mixtures: Application to rapid creep and stress amplification in subduction zone melange. *Geophysical Research Letters*, *46*(1), 169–178. https://doi.org/10.1029/2018GL081252

Birren, T., & Reber, J. E. (2019). The impact of rheology on the transition from stick-slip to creep in a semibrittle analog. *Journal of Geophysical Research: Solid Earth*, *124*, 3144–3154. https://doi.org/10.1029/2018JB016914

Brodsky, E. E., & Kanamori, H. (2001). Elastohydrodynamic lubrication of faults. *Journal of Geophysical Research*, *106*(B8), 16,357–16,374. https://doi.org/10.1029/2001JB000430

Cates, M. E., Wittmer, J. P., Bouchaud, J. P., & Claudin, P. (1998). Jamming, force chains, and fragile matter. *Physical Review Letters*, *81*(9), 1841–1844. https://doi.org/10.1103/PhysRevLett.81.1841

Clark, A. H., Kondic, L., & Behringer, R. P. (2012). Particle scale dynamics in granular impact. *Physical Review Letters*, *109*, 238302. https://doi.org/10.1103/PhysRevLett.109.238302

Cordonnier, B., Caricchi, L., Pistone, M., Castro, J., Hess, K. U., Gottschaller, S., et al. (2012). The viscous-brittle transition of crystal-bearing silicic melt: Direct observation of magma rupture and healing. *Geology*, *40*(7), 611–614. https://doi.org/10.1130/G3914.1

Daniels, K. E., & Hayman, N. W. (2008). Force chains in seismogenic faults visualized with photoelastic granular shear experiments. *Journal of Geophysical Research*, *113*, B11411. https://doi.org/10.1029/2008JB005781

Daniels, K. E., & Hayman, N. W. (2009). Boundary conditions and event scaling of granular stick-slip events. In M. Nakagawa, & S. Luding (Eds.), eds.*Powders and grains 2009* (Vol. 1145, pp. 567–570). New York: American Institute of Physics.

Daniels, K. E., Kollmer, J. E., & Puckett, J. G. (2017). Photoelastic force measurements in granular materials. *Review of Scientific Instruments*, *88*(5), 051808. https://doi.org/10.1063/1.4983049

Deubelbeiss, Y., Kaus, B. J. P., Connolly, J. A. D., & Caricchi, L. (2011). Potential causes for the non-Newtonian rheology of crystal-bearing magmas. *Geochemistry, Geophysics, Geosystems*, *12*, Q05007. https://doi.org/10.1029/2010GC003485

Evans, B., Fredrich, J. T., & Wong, T.-F. (1990). *The brittle-ductile transition in rocks: Recent experimental and theoretical progress*: *Geophysical Monograph Series* (Vol. 56, pp. 1–20). Washington, DC: American Geophysical Union.

Fagereng, A., & Sibson, R. H. (2010). Melange rheology and seismic style. *Geology*, *38*(8), 751–754. https://doi.org/10.1130/G30868.1

Frocht, M. M. (1941). *Photoelasticity* (Vol. 1). New York: University of Michigan, John Wiley & Sons.

Geminard, J. C., Losert, W., & Gollub, J. P. (1999). Frictional mechanics of wet granular material. *Physical Review E*, *59*(5), 5881–5890. https://doi.org/10.1103/PhysRevE.59.5881

Goren, L., Aharonov, E., Sparks, D., & Toussaint, R. (2011). The mechanical coupling of fluid-filled granular material under shear. *Pure and Applied Geophysics*, *168*(12), 2289–2323. https://doi.org/10.1007/s00024-011-0320-4

Handy, M. R. (1990). The solid-state flow law of polymineralic rocks. *Journal of Geophysical Research*, *95*(B6), 8647–8661. https://doi.org/10.1029/JB095iB06p08647

Handy, M. R. (1994). Flow laws for rocks containing 2 nonlinear viscous phases—A phenomenological approach. *Journal of Structural Geology*, *16*(3), 287–301. https://doi.org/10.1016/0191-8141(94)90035-3

Hayman, N. W., & Lavier, L. L. (2014). The geologic record of deep episodic tremor and slip. *Geology*, *42*(3), 195–198. https://doi.org/10.1130/G34990.1

Healy, D., Rizzo, R. E., Cornwell, D. G., Farrell, N. J. C., Watkins, H., Timms, N. E., et al. (2017). FracPaQ: A MATLAB™ toolbox for the quantification of fracture patterns. *Journal of Structural Geology*, *95*, 1–16. https://doi.org/10.1016/j.jsg.2016.12.003

Hecht, E., & Zajac, A. (1974). *Optics*. New York: Reading, Mass, Wiley.

Herrmann, H. J., Hovi, J.-P., & Luding, S. (1997). *Physics of dry granular media*. London: Springer.

Higashi, N., & Sumita, I. (2009). Experiments on granular rheology: Effects of particle size and fluid viscosity. *Journal of Geophysical Research*, *114*, B04413. https://doi.org/10.1029/2008JB005999
Holyoke, C. W., & Tullis, J. (2006). Formation and maintenance of shear zones. *Geology*, *34*(2), 105–108. https://doi.org/10.1130/G22116.1
Hooke, R. L. (1968). Model geology: Prototype and laboratory streams: Discussion. *GSA Bulletin*, *79*(3), 391–394. https://doi.org/10.1130/0016-7606(1968)79[391:MGPALS]2.0.CO;2
Howell, D., Behringer, R. P., & Veje, C. (1999). Stress fluctuations in a 2D granular Couette experiment: A continuous transition. *Physical Review Letters*, *82*(26), 5241–5244. https://doi.org/10.1103/PhysRevLett.82.5241
Huang, N., Ovarlez, G., Bertrand, F., Rodts, S., Coussot, P., & Bonn, D. (2005). Flow of wet granular materials. *Physical Review Letters*, *94*, 028301. https://doi.org/10.1103/PhysRevLett.94.028301
Iikawa, N., Bandi, M. M., & Katsuragi, H. (2016). Sensitivity of granular force chain orientation to disorder-induced metastable relaxation. *Physical Review Letters*, *116*, 128001. https://doi.org/10.1103/PhysRevLett.116.128001
Iverson, R. M., Reid, M. E., Iverson, N. R., LaHusen, R. G., Logan, M., Mann, J. E., & Brien, D. L. (2000). Acute sensitivity of landslide rates to initial soil porosity. *Science*, *290*(5491), 513–516. https://doi.org/10.1126/science.290.5491.513
Jaeger, H. M., Nagel, S. R., & Behringer, R. P. (1996). Granular solids, liquids, and gases. *Reviews of Modern Physics*, *68*(4), 1259–1273. https://doi.org/10.1103/RevModPhys.68.1259
Jammes, S., Lavier, L. L., & Reber, J. E. (2015). Localization and delocalization of deformation in a bimineralic material. *Journal of Geophysical Research: Solid Earth*, *120*, 3649–3663. https://doi.org/10.1002/2015JB011890
Jang, J. Y., & Khonsari, M. M. (2005). On the granular lubrication theory. Proceedings of the Royal Society A: Mathematical Physical and Engineering Sciences, v. *461*(2062), p. 3255–3278, https://doi.org/10.1098/rspa.2005.1510
Ji, S. C. (2004). A generalized mixture rule for estimating the viscosity of solid-liquid suspensions and mechanical properties of polyphase rocks and composite materials. *Journal of Geophysical Research*, *109*, B10207. https://doi.org/10.1029/2004JB003124
Jordan, P. (1988). The rheology of polymineralic rocks—An approach. *Geologische Rundschau*, *77*(1), 285–294. https://doi.org/10.1007/BF01848690
Jordan, P. G. (1987). The deformation behavior of bimineralic limestone halite aggregates. *Tectonophysics*, *135*(1–3), 185–197. https://doi.org/10.1016/0040-1951(87)90160-0
Ju, Y., Ren, Z., Mao, L., & Chiang, F.-P. (2018). Quantitative visualisation of the continuous whole-field stress evolution in complex pore structures using photoelastic testing and 3D printing methods. *Optics Express*, *26*(5), 6182–6201. https://doi.org/10.1364/OE.26.006182
Kennedy, T. (2006). Compact packings of the plane with two sizes of discs. *Discrete & Computational Geometry*, *35*(2), 255–267. https://doi.org/10.1007/s00454-005-1172-4
Kullback, S., & Leibler, R. A. (1951). On information and sufficiency. *Annals of Mathematical Statistics*, *22*(1), 79–86. https://doi.org/10.1214/aoms/1177729694
Lavier, L. L., Bennett, R. A., & Duddu, R. (2013). Creep events at the brittle ductile transition. *Geochemistry, Geophysics, Geosystems*, *14*, 3334–3351. https://doi.org/10.1002/ggge.20178
Lejeune, A. M., & Richet, P. (1995). Rheology of crystal-bearing melts - an experimental-study ay high viscosities. *Journal of Geophysical Research*, *100*(B3), 4215–4229. https://doi.org/10.1029/94JB02985
Li, L., Addad, A., Weidner, D., Long, H. B., & Chen, J. H. (2007). High pressure deformation in two-phase aggregates. *Tectonophysics*, *439*(1–4), 107–117. https://doi.org/10.1016/j.tecto.2007.04.004
Liu, C. H., Nagel, S. R., Schecter, D. A., Coppersmith, S. N., Majumdar, S., Narayan, O., & Witten, T. A. (1995). Force fluctuation in bead packs. *Science*, *269*(5223), 513–515. https://doi.org/10.1126/science.269.5223.513
Mahabadi, N., & Jang, J. (2017). The impact of fluid flow on force chains in granular media. *Applied Physics Letters*, *110*, 041907. https://doi.org/10.1063/1.4975065
Majmudar, T. S., & Behringer, R. P. (2005). Contact force measurements and stress-induced anisotropy in granular materials. *Nature*, *435*(7045), 1079–1082. https://doi.org/10.1038/nature03805
Maliva, R. G. (2016). *Borehole drilling and well construction, aquifer characterization techniques*: *Schlumberger Methods in Water Resources Evaluation Series* (Vol. 4, pp. 127–170). Switzerland: Springer.
Mancktelow, N. S. (2008). Interaction between brittle fracture and ductile flow during crustal deformation. *Bollettino della Societa Geologica Italiana*, *127*(2), 217–220.
Montesi, L. G. J. (2013). Fabric development as the key for forming ductile shear zones and enabling plate tectonics. *Journal of Structural Geology*, *50*, 254–266. https://doi.org/10.1016/j.jsg.2012.12.011
Osborn, S. G., Vengosh, A., Warner, N. R., & Jackson, R. B. (2011). Methane contamination of drinking water accompanying gas-well drilling and hydraulic fracturing. *Proceedings of the National Academy of Sciences of the United States of America*, *108*(20), 8172–8176. https://doi.org/10.1073/pnas.1100682108
Paola, C., Straub, K., Mohrig, D., & Reinhardt, L. (2009). The "unreasonable effectiveness" of stratigraphic and geomorphic experiments. *Earth-Science Reviews*, *97*(1–4), 1–43. https://doi.org/10.1016/j.earscirev.2009.05.003
Pec, M., Stunitz, H., Heilbronner, R., & Drury, M. (2016). Semi-brittle flow of granitoid fault rocks in experiments. *Journal of Geophysical Research: Solid Earth*, *121*, 1677–1705. https://doi.org/10.1002/2015JB012513
Peters, J. F., Muthuswamy, M., Wibowo, J., & Tordesillas, A. (2005). Characterization of force chains in granular material. *Physical Review E*, *72*, 041307. https://doi.org/10.1103/PhysRevE.72.041307
Puckett, J. G., 2012, State variables in granular materials: An investigation of volume and stress fluctuations. Ph.D.: North Carolina State University.
Radjai, F., Jean, M., Moreau, J. J., & Roux, S. (1996). Force distributions in dense two-dimensional granular systems. *Physical Review Letters*, *77*(2), 274–277. https://doi.org/10.1103/PhysRevLett.77.274
Randolph-Flagg, J., & Reber, J. E. (2020). Effect of grain size and grain size distribution on slip dynamics: An experimental analysis. *Tectonophysics*, *774*, 228288. https://doi.org/10.1016/j.tecto.2019.228288
Reber, J. E., Cooke, M. L., & Dooley, T. P. (2020). What model material to use? A review on rock analogs for structural geology and tectonics. *Earth-Science Reviews*, *202*, 1–21.
Reber, J. E., Hayman, N. W., & Lavier, L. L. (2014). Stick-slip and creep behavior in lubricated granular material: Insights into the brittle-ductile transition. *Geophysical Research Letters*, *41*, 3471–3477. https://doi.org/10.1002/2014GL059832
Reber, J. E., Lavier, L. L., & Hayman, N. W. (2015). Experimental demonstration of a semi-brittle origin for crustal strain transients. *Nature Geoscience*, *8*(9), 712–715. https://doi.org/10.1038/ngeo2496
Roscoe, R. (1952). The viscosity of suspended rigid spheres. *British Journal of Applied Physics*, *3*(8), 267–269. https://doi.org/10.1088/0508-3443/3/8/306

Ross, J. V., Bauer, S. J., & Hansen, F. D. (1987). Textural evolution of synthetic anhydrite halite mylonites. *Tectonophysics*, *140*(2–4), 307–326. https://doi.org/10.1016/0040-1951(87)90237-X

Sibson, R. H. (1996). Structural permeability of fluid-driven fault-fracture meshes. *Journal of Structural Geology*, *18*(8), 1031–1042. https://doi.org/10.1016/0191-8141(96)00032-6

Soeder, D. J. (2018). The successful development of gas and oil resources from shales in North America. *Journal of Petroleum Science and Engineering*, *163*, 399–420. https://doi.org/10.1016/j.petrol.2017.12.084

Uenishi, K., & Goji, T. (2018). Dynamic fracture and wave propagation in a granular medium: A photoelastic study. In Sedmak, A., Radakovic, Z., & Rakin, M. (Eds.), *Ecf22—Loading and environmental effects on structural integrity* (Vol. 13, pp. 769–774). Elsevier.

Webber, S., Ellis, S., & Fagereng, A. (2018). Virtual shear box experiments of stress and slip cycling within a subduction interface melange. *Earth and Planetary Science Letters*, *488*, 27–35. https://doi.org/10.1016/j.epsl.2018.01.035

Weijermars, R. (1986). Flow behaviour and physical chemistry of bouncing putties and related polymers in view of tectonic laboratory applications. *Tectonophysics*, *124*(3-4), 325–358. https://doi.org/10.1016/0040-1951(86)90208-8